

Article

Temperature Load Mode of Bridge in Permafrost Region of Qinghai–Tibet Railway

Bin Yan ^{1,2}, Ruiqi Cheng ¹ , Haoran Xie ³  and Xiangmin Zhang ^{1,*}

¹ School of Civil Engineering, Central South University, Changsha 410075, China; binyan@csu.edu.cn (B.Y.); crq1205@csu.edu.cn (R.C.)

² National Engineering Research Center of High-Speed Railway Construction Technology, Changsha 410075, China

³ China Railway Design Corporation, Tianjin 300308, China; xiehaoran@crdc.com

* Correspondence: zxmzk6298@csu.edu.cn

Abstract: The Qinghai–Tibet railway is the plateau permafrost railway with the highest altitude and the longest line in the world. The natural conditions along the line are harsh, with many unfavorable factors such as low temperature, strong ultraviolet radiation, and large changes in daily temperature, resulting in frequent bridge damage. In order to study the bridge temperature field and its effect in the permafrost region of the Qinghai–Tibet railway, a long-term field test was carried out, and a calculation model of sunshine temperature field of concrete two-piece T-beam was established based on the principle of meteorology and heat transfer. On this basis, the beam temperature difference load mode, beam section temperature distribution law, and temperature effect were obtained. As revealed, the daily temperature difference of the Qinghai–Tibet railway bridge is large in winter, which is related to the ground’s effective radiation and surface reflectivity, and the maximum value has exceeded the current codes. The beam section temperature field shows “internal heat and external cold” in the morning and “internal cold and external heat” from noon to evening. Under the action of strong radiation and large temperature difference, bridge displacement occurs frequently, by which it is easy to cause damage to rail fasteners and bridge bearings. Based on the field test and finite element analysis, the bridge temperature difference load mode was proposed, which makes up for the deficiency that the relevant codes do not consider the plateau’s special climatic conditions and can provide a reference for the construction of plateau railways such as the Sichuan–Tibet railway.

Keywords: Qinghai–Tibet railway; concrete bridge; temperature field; finite element; heat transfer; experimental study



Citation: Yan, B.; Cheng, R.; Xie, H.; Zhang, X. Temperature Load Mode of Bridge in Permafrost Region of Qinghai–Tibet Railway. *Appl. Sci.* **2022**, *12*, 4377. <https://doi.org/10.3390/app12094377>

Academic Editors:
Szymon Wojciechowski,
Antoine Ferreira
and Krzysztof Talaśka

Received: 11 April 2022

Accepted: 25 April 2022

Published: 26 April 2022

Publisher’s Note: MDPI stays neutral with regard to jurisdictional claims in published maps and institutional affiliations.



Copyright: © 2022 by the authors. Licensee MDPI, Basel, Switzerland. This article is an open access article distributed under the terms and conditions of the Creative Commons Attribution (CC BY) license (<https://creativecommons.org/licenses/by/4.0/>).

1. Introduction

The Qinghai–Tibet railway is one of China’s four major projects in the new century and the first railway to the hinterland of Tibet. It is world-famous for overcoming extreme conditions such as severe cold on the plateau, lack of oxygen, fragile ecology, and frozen soil (Figure 1). The Golmud–Lhasa section of the Qinghai–Tibet railway passes through Gobi deserts and marshes and across the Qinghai–Tibet Plateau, with a total mileage of 1142 km and about 550 km through continuous permafrost region. The average elevation of the whole line is about 4380 m, and the highest point of the railway crossing Tanggula Mountain is 5072 m above sea level. The natural conditions along the line are harsh, with many unfavorable factors such as severe cold, low atmospheric oxygen content, strong ultraviolet radiation, and large changes in daily temperature [1,2].

Due to the influence of complex plateau environment, especially strong solar radiation and significant daily temperature difference, all manner of bridge damage has appeared on the Qinghai–Tibet railway. In the field equipment inspection, it was found that the bridge damage in the Golmud–Lhasa section of the Qinghai–Tibet railway mainly manifested in the following aspects: direct contact of adjacent beams (Figure 2a), fracture of bearing limit

block (Figure 2b), displacement of bearing, bending of bearing bolt, deflection of pier and abutment, etc. The damage and excessive deformation of the bridge structure will lead to the irregularity of the line, affect the driving stability and comfort, and even threaten the operational safety of the train. Therefore, it is urgent to study the temperature load mode of the concrete bridge in the permafrost region of the Qinghai–Tibet railway, explore the deformation and damage mechanism of the bridge-track structure, and provide a scientific basis for the design and maintenance of CWR (Continuously Welded Rail) on the bridge in the plateau area.



Figure 1. Permafrost region of Qinghai–Tibet railway.



Figure 2. Bridge damage of Qinghai–Tibet railway. (a) Direct contact of adjacent beams. (b) Fracture of bearing limit block.

In the design of CWR on the bridge in China, when calculating the expansion force of concrete bridges with ballasted track caused by temperature difference, the maximum daily temperature difference of the beam body is taken as 15 °C [3]. As the temperature in the permafrost region of the Qinghai–Tibet railway and the conditions for the bridge to receive sunshine are different from those in other areas, it is still unclear whether the value of the beam's daily temperature difference in the code is applicable. Domestic and foreign scholars have conducted plentiful research on the temperature field and temperature effect on the bridge structure under the action of solar radiation. The main research methods include the experimental research method [4–9], theoretical analysis method [10–15], finite element software analysis method [16–21], and a research method combining the above methods [22–27]. For instance, Xiao L conducted long-term monitoring of a prestressed concrete box girder bridge, established the solar radiation boundary condition and transverse temperature gradient prediction model based on the measured data, and calculated the longitudinal and transverse tensile stress of the bridge structure [8]. Song Z. proposed a new method to determine the effect of solar radiation based on the stationary binomial probability model of random process and obtained the design standard values of equivalent

linear temperature difference and cross-section temperature difference of high-performance concrete box girder in the design reference period [12]. Song X. studied the influence of solar temperature gradient on long-span concrete box girder bridge during construction by using ANSYS software [17]. Lou P. proposed a statistical method for establishing virtual distribution by using the reliability high moment theory and put forward the temperature action model suitable for bridge and track structures; the distribution law of uniform temperature spectrum was fitted by Fourier series, and the relationship between structure and atmospheric uniform temperature was established [25]. However, the above research is mostly aimed at specific bridge engineering examples and particular weather conditions, which is not suitable for the special geographical and climatic conditions of Qinghai–Tibet railway, and its application has great limitations. In some studies, the test cycle is short, makes it difficult to reflect the impact of climate conditions and date on the bridge temperature field, and there is a large error between the theoretical analysis results and the measured results. In short, the plateau’s adaptability of temperature load mode in existing research and codes is not clear, and the mechanical behavior characteristics of bridge and track structures under complex plateau climate conditions need to be explored. Therefore, it is necessary to carry out the research on the bridge temperature load mode according to the special climatic conditions along the Qinghai–Tibet railway, so as to provide support for the service safety of CWR on the bridge.

In order to study the temperature distribution characteristics and temperature effect of bridges in the permafrost area of Qinghai–Tibet railway, a long-term field test and finite element simulation analysis of the temperature field of the T-beam bridge in a representative section of the Qinghai–Tibet railway were carried out. Through one-year field monitoring, the variation laws of air temperature, beam temperature difference, and beam displacement were obtained. The heat exchange between the bridge and the outside world was transformed into heat flux boundary conditions, and the sunshine temperature field simulation model of the T-beam bridge of the Qinghai–Tibet railway was established based on the thermal analysis module of large-scale general finite element software ANSYS (Version: 19.2; ANSYS, Inc.; Canonsburg, PA, USA). The correctness of the finite element method was verified by the measured data. On this basis, the load mode of beam temperature difference and the temperature distribution law of the beam section in the permafrost area of the Qinghai–Tibet railway were analyzed, and the stress and displacement of the bridge and track under the action of beam temperature difference were studied. The temperature difference load mode proposed in this paper makes up for the deficiency that the relevant codes do not consider the special climatic conditions of the plateau. It can provide a reference for the design of CWR on a bridge in the plateau areas, such as the Sichuan–Tibet railway, and has strong engineering application value.

2. Test Scheme

Based on the long-term field test of representative sections in the permafrost region of the Qinghai–Tibet railway, the variation laws of air temperature, beam temperature, and beam-rail displacement were obtained. The accumulated large amount of measured data provides data basis and verification conditions for further study of bridge temperature load mode through finite element analysis.

2.1. Test Method

Since the Qinghai–Tibet railway has been completed and opened to traffic, the commonly used method of testing the internal temperature of the bridge through embedded temperature sensors has been difficult to achieve, so it can only test the surface temperature of the bridge. The surface temperature sensors are pasted on the inner and outer surfaces of the beam using thermal conductive adhesive with good thermal conductivity. The typical bridge structure of the Qinghai–Tibet railway is the concrete double-piece T-shaped, simply supported beam bridge, and the test diagram is shown in Figure 3.

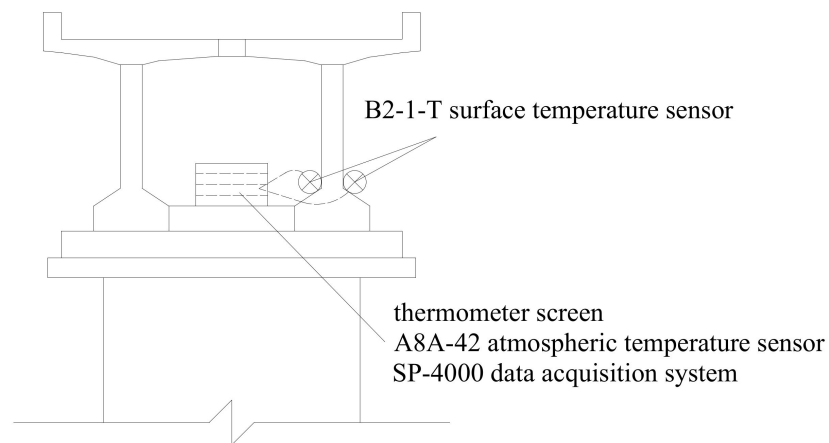


Figure 3. Schematic diagram of beam surface temperature test.

The displacement sensor is fixed at the rail above the fixed support of the bridge, and the sensor reading is the beam-rail longitudinal relative displacement (Figure 4b). When the longitudinal displacement sensor is installed at the beam gap, the telescopic displacement of the sensor is the displacement of the beam end (Figure 4c).

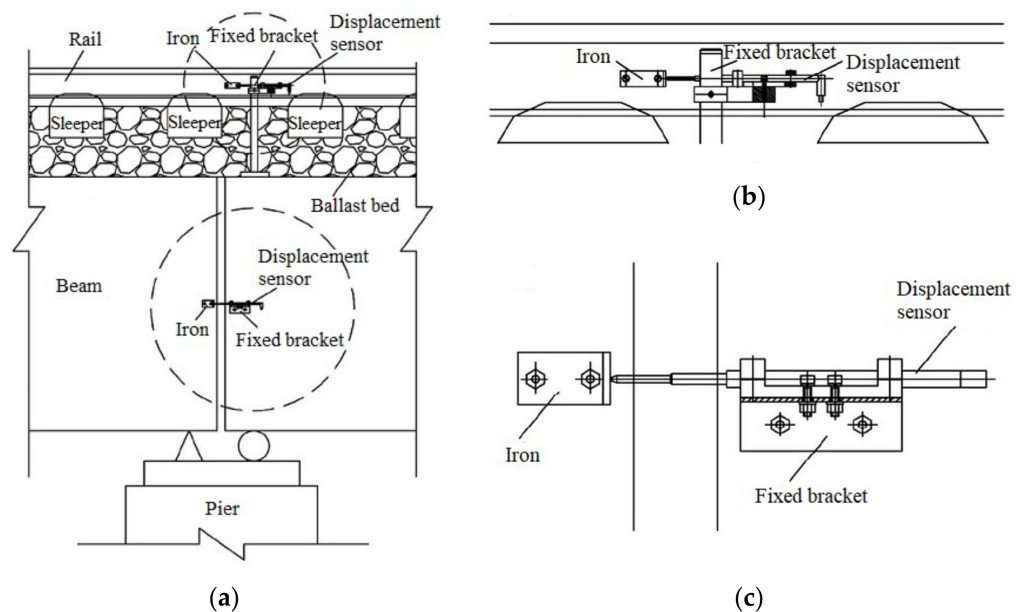


Figure 4. Schematic diagram of displacement test. (a) General layout. (b) Test method for beam-rail longitudinal relative displacement. (c) Test method for beam end longitudinal displacement.

2.2. Test System Composition, Layout, and Verification

The beam temperature monitoring system is composed of surface temperature sensor, atmospheric temperature sensor, data acquisition and storage system, control analysis software, thermometer, instrument shelter, etc., as shown in Figure 5.

The beam and rail longitudinal displacement monitoring system is mainly composed of data acquisition memory, control analysis software, displacement sensor, instrument shelter, battery, solar panel, etc., as shown in Figure 6.

In the permafrost region of the Qinghai–Tibet railway, the test systems are arranged on the railway bridge at the place with representative climate and environment. The specific layout scheme is shown in Table 1.

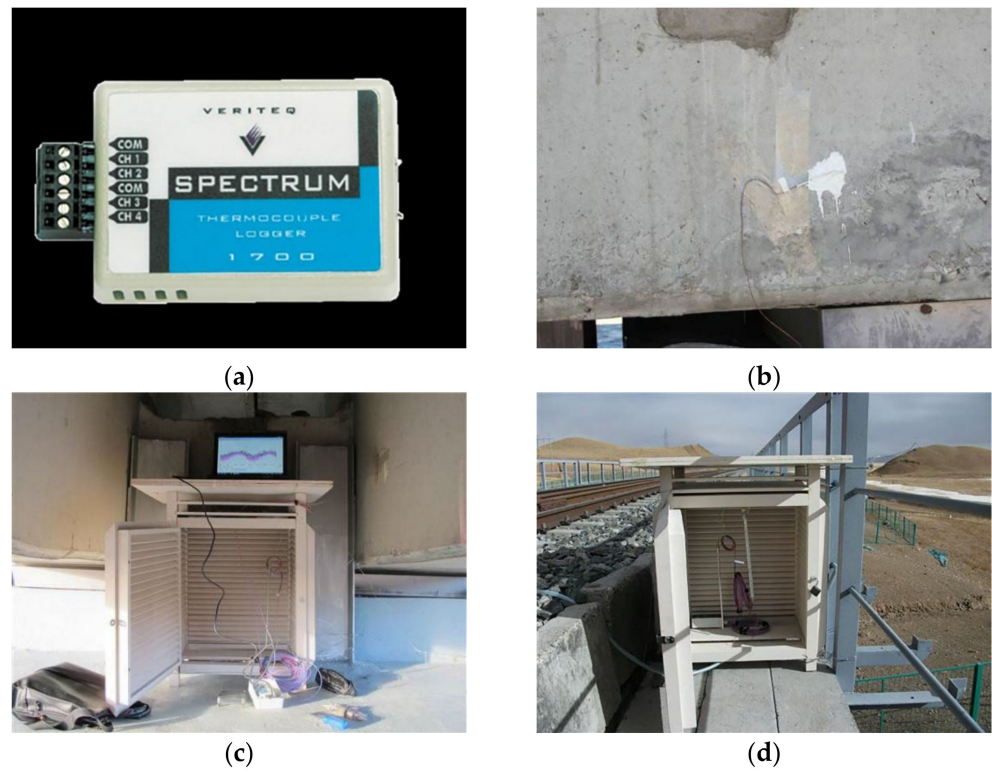


Figure 5. Beam temperature monitoring system. (a) Data acquisition system. (b) Surface temperature sensor. (c) Instrument shelter. (d) Atmospheric temperature sensor.

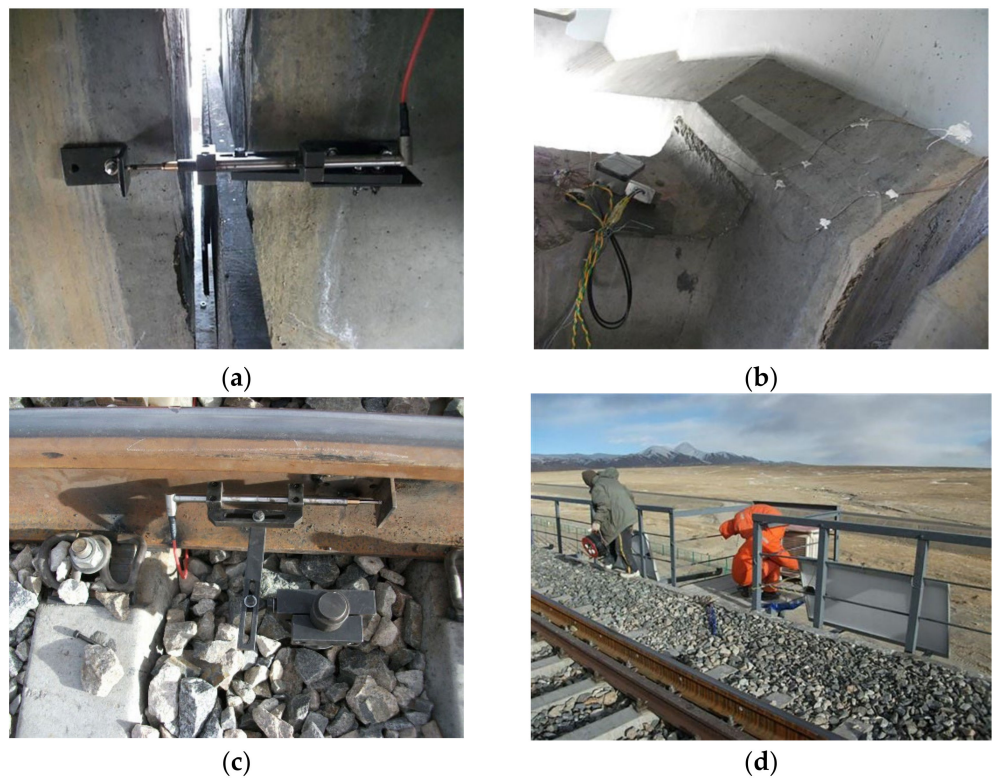


Figure 6. Beam and rail longitudinal displacement monitoring system. (a) Displacement sensor. (b) Beam end displacement observation. (c) Beam-rail longitudinal relative displacement observation. (d) Solar panel placed on bridge guardrail.

Table 1. Test instrument layout scheme.

Layout Location	Railway Mileage	Test System	Monitoring Content
Budongquan	K978	Beam temperature monitoring system, beam-rail displacement monitoring system	Air temperature, beam temperature, beam end displacement and beam-rail longitudinal relative displacement
Tuotuohe	K1243	Beam temperature monitoring system	Air temperature, beam temperature
Za'gya Zangbo	K1450	Beam temperature monitoring system	Air temperature, beam temperature

In order to verify the reliability of the temperature test system, the rail temperature was manually tested for 24 h at a buffer zone of the Budongquan CWR test section. The manual test time is the same as the system sampling time, and the test data are shown in Figure 7. The manual test data are relatively close to the data collected by the system, indicating that the temperature test system has good reliability. When verifying the reliability of the displacement test system, the beam gap width was manually tested for 24 h with a Vernier caliper at the corresponding position where the longitudinal displacement sensor is installed. The daily variation law of the beam gap is shown in Figure 8. It can be seen from the figure that the average value of the difference between manual test and system test results is 0.07 mm, and the standard deviation is 0.18 mm, showing good consistency.

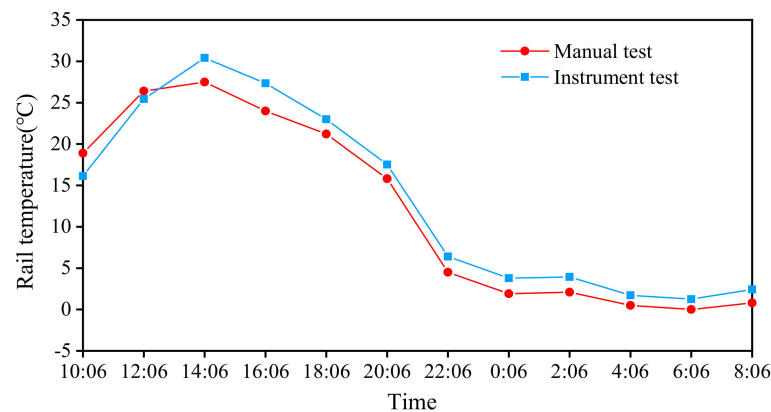


Figure 7. Comparison of rail temperature test results.

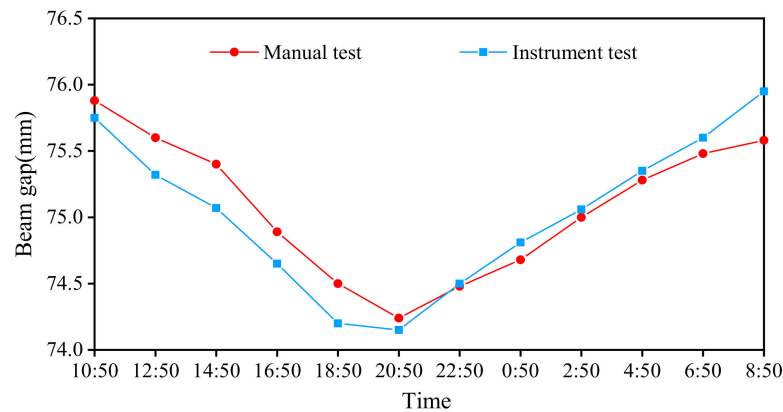


Figure 8. Comparison of beam gap width test results.

3. Test Result

Through long-term monitoring, a large amount of temperature and displacement data were obtained. On this basis, the distribution laws of daily beam temperature difference, beam end displacement, and beam-rail relative displacement were studied.

3.1. Monitoring Results and Analysis of Beam Temperature

Temperature monitoring was carried out in the Tuotuohe and Za'gya Zangbo regions for a period of one year, and the sampling interval of the beam temperature monitoring system was set at 2 h. According to the measured beam surface temperature at different times, the daily beam temperature difference was calculated as shown in Figures 9 and 10.

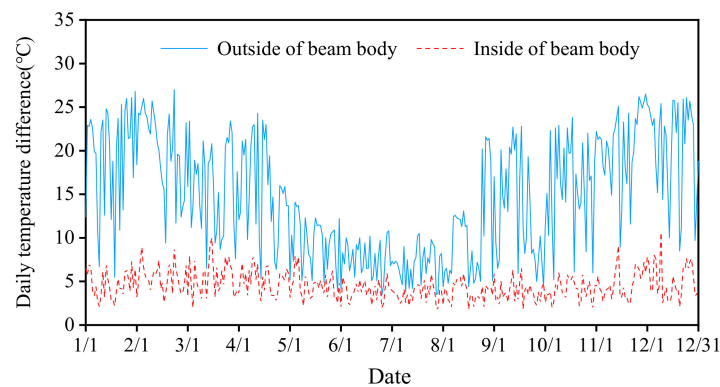


Figure 9. Measured daily beam temperature difference in Tuotuohe region.

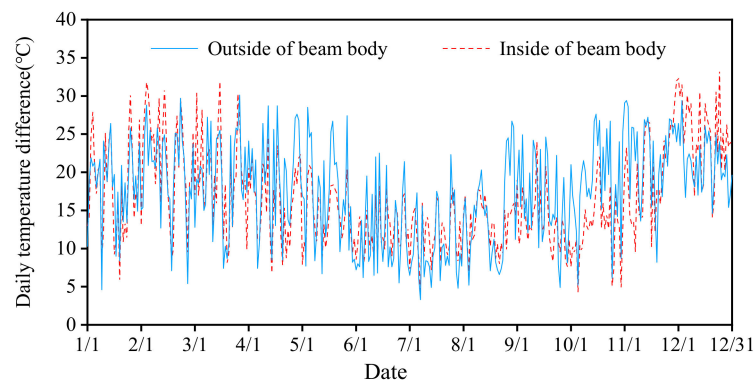


Figure 10. Measured daily beam temperature difference in Za'gya Zangbo region.

It can be seen from Figure 9 to Figure 10 that the daily temperature difference on the beam surface presents a large value in winter and a small value in summer, which is similar to the variation law of air temperature difference. The maximum daily temperature difference inside the beam body in Tuotuohe and Za'gya Zangbo region reaches 11.1 °C and 33.3 °C, respectively, and the maximum daily temperature difference outside the beam body reaches 27.0 °C and 30.1 °C, respectively, which is far greater than the standard value of 15 °C.

Since only the surface temperature of the bridge can be measured, and the daily temperature difference of the bridge cannot be precisely reflected, it is necessary to accurately analyze the temperature field distribution of the cross-section of the beam through finite element software.

3.2. Monitoring Results and Analysis of Beam-Rail Longitudinal Displacement

The longitudinal displacement monitoring of beam and rail was carried out in the Budongquan region for 7 months, and the system's automatic acquisition interval was 2 h. The monitoring results are sorted as shown in Figure 11.

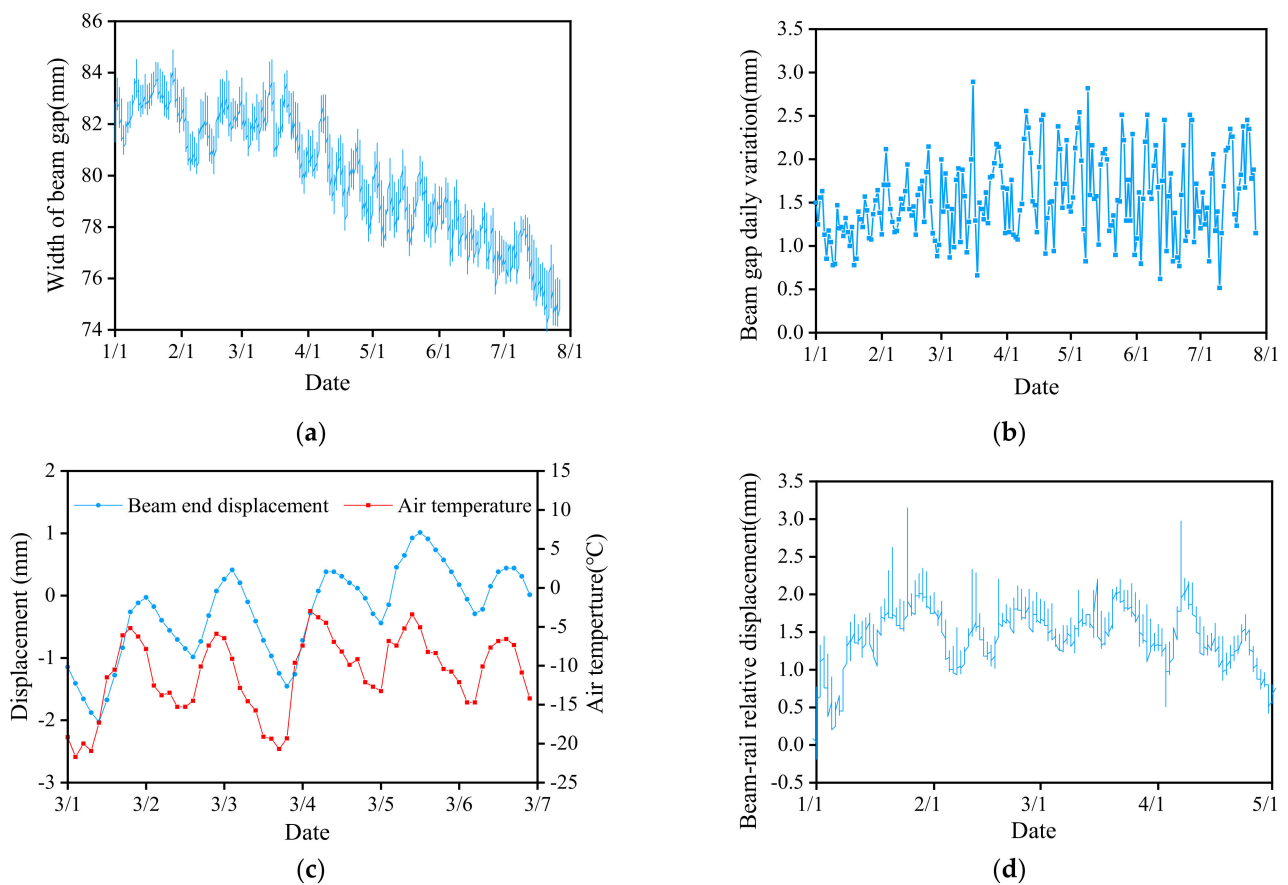


Figure 11. Longitudinal displacement of beam and rail. (a) Width of beam gap. (b) Daily variation in beam end displacement. (c) Relationship between beam end displacement and temperature change. (d) Beam-rail longitudinal relative displacement.

As can be seen from Figure 11, the beam end displacement changes periodically with the daily air temperature, but lags behind the air temperature for about 2 h, which is related to the poor thermal conductivity of the concrete. The displacement of the beam end changes greatly in spring, and the maximum daily displacement is 2.89 mm (16 March). During the observation period, the cumulative relative displacement of the beam and rail is 1.18 mm, and the maximum daily variation is 1.43 mm (25 January). The cumulative change in beam gap width is 7.00 mm, and the displacement continues to increase with time. This monitoring result provides strong evidence for the frequent occurrence of direct contact of adjacent beams, bridge bearing failure, and other damage in the permafrost region of the Qinghai–Tibet railway. The reason for the damage to these bridges is that the daily temperature difference in this area is large, resulting in frequent telescopic displacement of the beam, and the performance of the bearing cannot meet the requirements of frequent displacement of the beam.

4. Finite Element Model

Based on the general finite element software ANSYS, the analysis model of the sunshine temperature field of the concrete two-piece T-beam was established, and the accuracy of the analysis method was verified by the measured data.

4.1. Sunshine Temperature Field Simulation Model

The geological and climatic conditions of the Qinghai–Tibet Plateau are complex, and the concrete bridge structure exposed to the air must be closely related to the surrounding natural environment. Existing studies show that the temperature change of the bridge

beam is related to the geographical location, topographic conditions, the orientation of the bridge, season, solar radiation intensity, and temperature change.

Since the geographic latitude and longitude spanned by the bridge is very small, and the temperature distribution along the length of the bridge is relatively close, theoretically, there is no heat conduction process along the longitudinal direction of the bridge, and the slight change in the temperature difference along the length of the bridge can be ignored. Therefore, the temperature field of bridge structure can be simplified as a 2D transient nonlinear problem on the section. The heat exchange between the bridge and the outside world can be divided into three parts: solar radiation, radiation heat transfer, and convection heat transfer. Based on the thermal analysis module of large-scale general finite element software ANSYS, these three heat exchange actions were transformed into heat flux boundary conditions, and the calculation model of sunshine temperature field distribution of double-piece T-beam bridge of Qinghai–Tibet railway was established, as shown in Figure 12 [28].

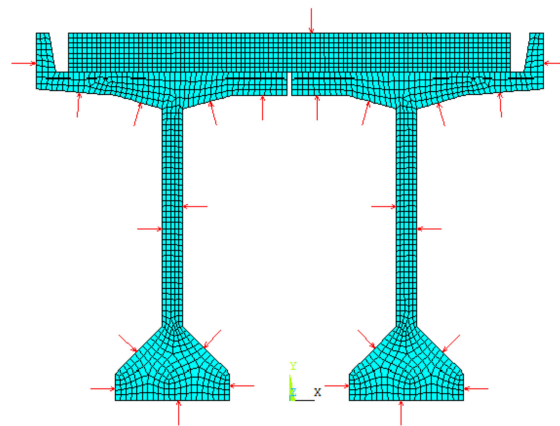


Figure 12. Sunshine temperature field simulation model.

According to relevant literature [29–32], the specific heat capacity of concrete is $920 \text{ J}/(\text{kg}\cdot\text{K})$, the thermal conductivity is $1.74 \text{ W}/(\text{m}^2\cdot\text{K})$, the unit weight of concrete is $2400 \text{ kg}/\text{m}^3$, the radiation absorption coefficient of the concrete surface is 0.65, the average reflectivity of snow covered ground is 0.7, the blackness of the radiation system between the outer surface of T-beam and sky radiation surface and ground is 0.9, and the atmospheric blackness is 0.8.

4.2. Model Validation

The air temperature and beam temperature collected in the field test were used as boundary conditions for progressive loading, and the temperature field distribution of the beam section at different times was calculated. By comparing the measured data of temperature sensor in Tuotuohe region with the results of corresponding nodes calculated by finite element method (Table 2), it was found that the temperature values are basically consistent, thereby determining the correctness and reliability of this model.

Table 2. Comparison between finite element calculation results and measured data.

Time	Position	Finite element Calculation Results ($^{\circ}\text{C}$)	Measured Data ($^{\circ}\text{C}$)	Error of Calculation
7/31-5:00	Internal measuring point	6.59	6.60	0.15%
	Outer measuring point	6.13	6.10	0.49%
7/31-19:00	Internal measuring point	9.63	10.20	5.60%
	Outer measuring point	11.81	12.10	2.40%

5. Finite Element Analysis Results

Using the established bridge sunshine temperature field model, the distribution law of bridge temperature field was analyzed. Combined with the measured data, the bridge temperature difference load mode suitable for the permafrost region of the Qinghai–Tibet railway was proposed.

5.1. Distribution Law of Beam Temperature Difference

The daily temperature difference of the beam calculated by the finite element model is shown in Figure 13.

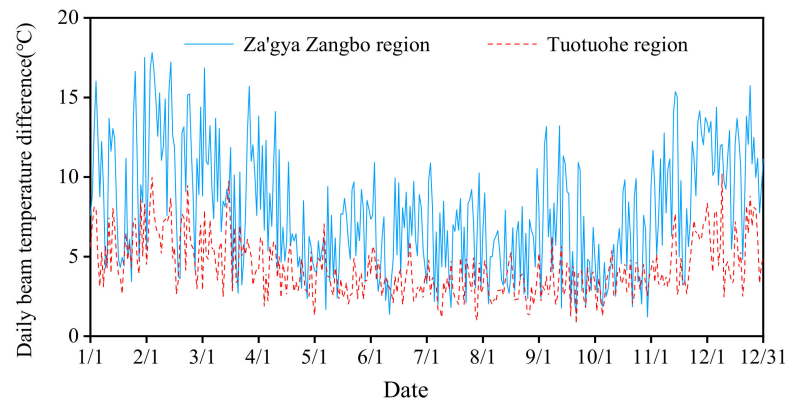


Figure 13. Beam temperature difference calculated by finite element software.

According to ANSYS thermal analysis, the maximum daily beam temperature difference in the Tuotuohe region is 10.2 °C, and the maximum daily beam temperature difference in Za'gya Zangbo region is 17.8 °C, which exceeds the value of 15 °C specified in *Code for Design of Railway Continuously Welded Rail* [3]. The time when the beam daily temperature difference in Za'gya Zangbo region is greater than 15 °C is 20 days, accounting for 5.31% of the total number of samples, mainly from November to March of the second year.

The larger value of beam temperature difference appears in winter, which is mainly related to the ground's effective radiation and surface reflectivity. The ground effective radiation of the Qinghai–Tibet Plateau is large in autumn and spring and small in winter and summer [32]. The surface reflectance is smaller in summer, larger in winter, and the second largest in spring. In summer, the ground effective radiation and the surface reflectance are low, and the change in beam temperature difference is also low. In winter, the ground effective radiation appears to have a low value, but the surface reflectance appears to have a large value, so the change in beam temperature difference remains high.

Based on the measured data and heat transfer simulation analysis, the temperature difference load mode suitable for concrete two-piece T-beam in typical areas of Qinghai–Tibet railway is calculated, as shown in Table 3.

Table 3. Temperature difference load mode.

Season	Tuotuohe Region		Za'gya Zangbo Region	
	Daily Beam Temperature Difference (°C)	Daily Air Temperature Difference (°C)	Daily Beam Temperature Difference (°C)	Daily Air Temperature Difference (°C)
Spring	9.76	18.30	16.84	21.90
Summer	5.96	10.90	10.91	13.20
Autumn	8.35	17.10	15.36	21.30
Winter	10.19	20.50	17.81	23.00

5.2. Distribution Law of Temperature Field

In order to study the temperature distribution law of the beam section, the temperature at various positions of the beam section at different times of a day in winter in the Tuotuohe region is selected for analysis. The daily temperature variation law of the beam section is shown in Figure 14.

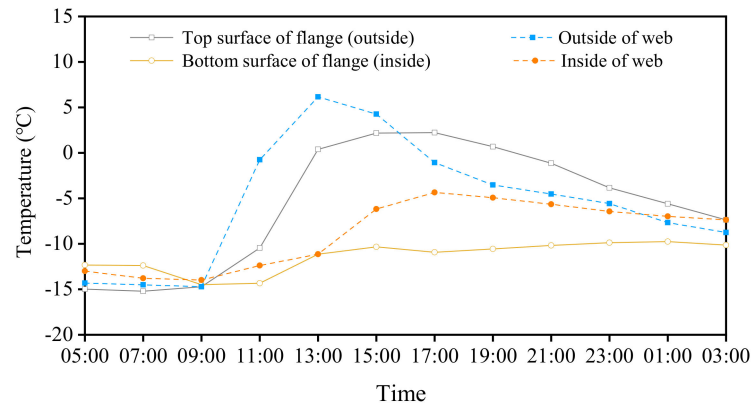


Figure 14. Diurnal variation in beam section temperature field in the Tuotuohe region.

It can be seen from Figure 14 that the bridge temperature field varies with the air temperature in a daily cycle, and the temperature variation rule of the flange plate and web of the bridge is basically consistent. Since the inner surface of the bridge is not directly affected by solar radiation, and the thermal conductivity of concrete is poor, the temperature change of the inner side is much smaller than that of the outer surface, and there is a certain lag. Therefore, from noon to night, when the external temperature rises, the temperature field of the beam section shows “internal cold and external heat”. From night to early morning, when the external temperature decreases, the temperature field of the beam section shows “internal heat and external cold”. From 11:00 to 15:00 every day, the solar radiation is strong, resulting in drastic changes in the beam temperature. Under the shielding effect of the track structure, the temperature change amplitude of upper flange is less than that of web. The variation in the bridge temperature field in other seasons is similar to that in winter, but the variation range is relatively small.

6. Temperature Effect Analysis

The simulation model of CWR on a five-span 32 m bridge was established by using ANSYS software, as shown in Figure 15. The beam adopts a double-piece T-shaped concrete simply supported beam of the Qinghai–Tibet railway, and the rail adopts a U75V60 rail. The fixed support is located on the left side of the simply supported beam, and 100 m long subgrade sections are set on both sides of the bridge span to eliminate the influence of the boundary. The beam-rail interaction model has been verified by the example in UIC 774-3. The daily temperature difference of the bridge is taken as 17.8 °C of the maximum daily beam temperature difference in the Za’gya Zangbo region. The stress and displacement distribution of the CWR on the bridge are shown in Figure 16.

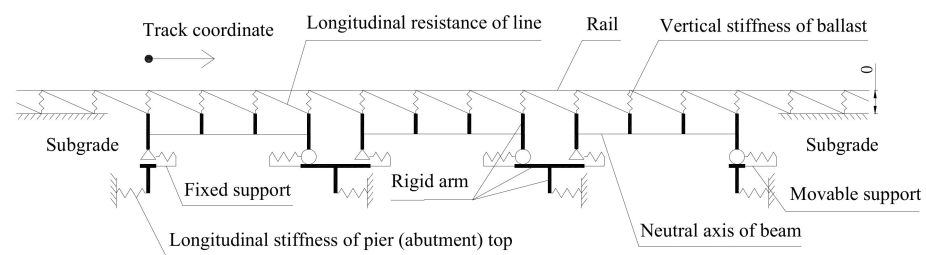


Figure 15. Mechanical model diagram of CWR on the bridge.

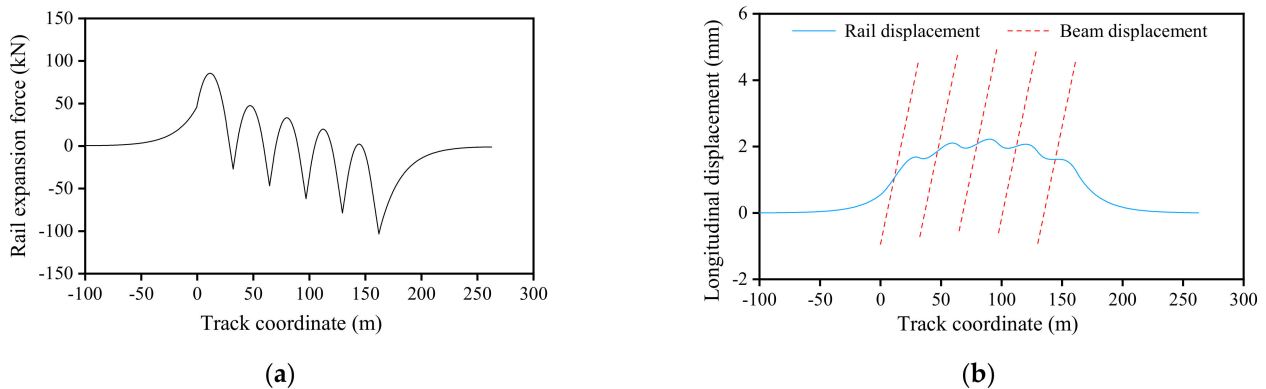


Figure 16. Stress and displacement of CWR on bridge. (a) Rail expansion force. (b) Bridge and rail displacement.

Since the fixed pier is located on the left end and the bridge expands and deforms to the right, the rail near the movable support of the right abutment bears the maximum additional temperature pressure of 103.3 kN, and the rail near the left abutment bears the maximum temperature tension of 85.5 kN. On each bridge span from left to right, the rail's additional pressure gradually increases and the additional tension gradually decreases, indicating that the beam-rail interaction caused by bridge expansion gradually accumulates to the right. The displacement distribution of each span bridge is almost the same, increasing linearly from the fixed end to the movable end, and the maximum longitudinal displacement is 5.0 mm. The maximum longitudinal displacement of the rail occurs in the middle of the bridge, and the displacement is 2.2 mm. The maximum relative displacement of beam and rail is 3.4 mm, which appears at the right abutment. It can be seen that under the conditions of strong radiation and large temperature difference in the Qinghai–Tibet railway area, the bridge produces frequent telescopic displacement, which can easily lead to the attenuation of the performance of rail fasteners and bridge bearings and has an adverse impact on the durability of track structure.

7. Conclusions

In order to study the temperature load mode of a railway bridge in the permafrost region of the Qinghai–Tibet railway, long-term experimental research and finite element simulation analysis were carried out in this paper. The main conclusions are as follows:

- (1) The daily temperature difference of a concrete two-piece T-beam bridge in the Qinghai–Tibet railway area presents a large value from November to March of the next year, which is mainly related to the ground's effective radiation and surface reflectivity.
- (2) The maximum daily temperature difference of the beam body in the Za'gya Zangbo region is 17.8 °C, exceeding the 15 °C specified in *Code for Design of Railway Continuously Welded Rail*. It is suggested that when designing bridges in plateau areas, the beam's temperature difference should be increased as appropriate to ensure the durability requirements of bridge in operation. In addition, observation and analysis should be further strengthened to provide important data support for revising and perfecting the codes.
- (3) Through long-term field test and simulation calculation, it is found that under the conditions of strong radiation and large daily temperature difference in the Qinghai–Tibet railway area, the bridge frequently produces telescopic displacement, which can easily lead to the attenuation of the performance of rail fasteners and bridge bearings and has an adverse impact on the safety of track structure. It is suggested that the maintenance of the bridge structure be strengthened and that performance index of bearing in this area be improved.
- (4) Based on the measured data and heat transfer simulation analysis, the temperature difference load mode suitable for concrete two-piece T-beams in typical areas of the

Qinghai–Tibet railway was proposed. This study overcomes the deficiency of regional limitations in the existing research, and makes up for the deficiency that the relevant codes do not consider the plateau’s special climatic conditions, which can provide a reference for the design of CWR on a bridge in the plateau. Furthermore, the temperature load modes of other types of bridges need to be further studied.

Author Contributions: Conceptualization, B.Y.; methodology B.Y. and X.Z.; software, B.Y., R.C., H.X. and X.Z.; validation, R.C., H.X. and X.Z.; formal analysis, R.C., H.X. and X.Z.; writing—original draft preparation, R.C. and X.Z.; writing—review and editing, B.Y. and R.C. All authors have read and agreed to the published version of the manuscript.

Funding: This research was funded by the National Key R&D Program of China (grant number 2017YFB1201204) and the Project of Science and Technology Research and Development Program of China National Railway Group (grant number K2021G026).

Institutional Review Board Statement: Not applicable.

Informed Consent Statement: Not applicable.

Data Availability Statement: All data, models, and code generated or used during the study appear in the submitted article.

Conflicts of Interest: The authors declare no conflict of interest.

References

1. Zhang, L.; Gao, L.; Zhao, L.; Chen, K. Spatial and temporal characteristics of global solar radiation over Qinghai-Tibetan plateau based on ITPCAS dataset. *Acta Energ. Sol. Sin.* **2019**, *40*, 2521–2529. (In Chinese)
2. Liu, F.; Chen, Q.; Zhang, Y.; Zhou, Q.; Li, C.; Cao, S. The characteristics of natural hazard regional combination law along the Qinghai-Tibet railway. *Sci. Geogr. Sin.* **2010**, *30*, 384–390. (In Chinese)
3. *TB10015-2012*; Chinese National Standards, Code for Design of Railway Continuously Welded Rail. China Railway Publishing House: Beijing, China, 2013. (In Chinese)
4. Fan, J.; Liu, Y.; Liu, C. Experiment study and refined modeling of temperature field of steel-concrete composite beam bridges. *Eng. Struct.* **2021**, *240*, 112350. [[CrossRef](#)]
5. Li, H.; Zhang, Z.; Deng, N. Temperature field and gradient effect of a steel-concrete composite box girder bridge. *Adv. Mater. Sci. Eng.* **2021**, *2021*, 9901801. [[CrossRef](#)]
6. Abid, S.; Mussa, F.; Tayşi, N.; Özakça, M. Experimental and finite element investigation of temperature distributions in concrete-encased steel girders. *Struct. Control Health Monit.* **2017**, *25*, e2042. [[CrossRef](#)]
7. Abid, S.; Tayşi, N.; Ozakca, M. Experimental analysis of temperature gradients in concrete box-girders. *Constr. Build. Mater.* **2016**, *106*, 523–532. [[CrossRef](#)]
8. Lei, X.; Fan, X.; Jiang, H.; Zhu, K.; Zhan, H. Temperature field boundary conditions and lateral temperature gradient effect on a PC box-girder bridge based on real-time solar radiation and spatial temperature monitoring. *Sensors* **2020**, *20*, 5261. [[CrossRef](#)] [[PubMed](#)]
9. Xiao, F.; Hulsey, J.; Balasubramanian, R. Fiber optic health monitoring and temperature behavior of bridge in cold region. *Struct. Control Health Monit.* **2017**, *24*, e2020. [[CrossRef](#)]
10. Zhu, J.; Meng, Q. Effective and fine analysis for temperature effect of bridges in natural environments. *J. Bridge Eng.* **2017**, *22*, 04017017. [[CrossRef](#)]
11. Tayşi, N.; Abid, S. Temperature distributions and variations in concrete box-girder bridges: Experimental and finite element parametric studies. *Adv. Struct. Eng.* **2015**, *18*, 469–486. [[CrossRef](#)]
12. Song, Z.; Xiao, J.; Shen, L. On temperature gradients in high-performance concrete box girder under solar radiation. *Adv. Struct. Eng.* **2012**, *15*, 399–415. [[CrossRef](#)]
13. Xue, J.; Lin, J.; Briseghella, B.; Tabatabai, H.; Chen, B. Solar radiation parameters for assessing temperature distributions on bridge cross-sections. *Appl. Sci.* **2018**, *8*, 627. [[CrossRef](#)]
14. Kennedy, J.; Soliman, M. Temperature distribution in composite bridges. *J. Struct. Eng.* **1987**, *113*, 475–482. [[CrossRef](#)]
15. Branco, F.; Mendes, P. Thermal actions for concrete bridge design. *J. Struct. Eng.* **1993**, *119*, 2313–2331. [[CrossRef](#)]
16. Sheng, X.; Yang, Y.; Zheng, W.; Zhou, B.; Li, S.; Huang, L. Study on the time-varying temperature field of small radius curved concrete box girder bridges. *AIP Adv.* **2020**, *10*, 105013. [[CrossRef](#)]
17. Song, X.; Melhem, H.; Li, J.; Xu, Q.; Cheng, L. Effects of solar temperature gradient on long-span concrete box girder during cantilever construction. *J. Bridge Eng.* **2016**, *21*, 4015061. [[CrossRef](#)]
18. Kim, S.; Park, S.; Wu, J.; Won, J. Temperature variation in steel box girders of cable-stayed bridges during construction. *J. Constr. Steel Res.* **2015**, *112*, 80–92. [[CrossRef](#)]

19. Zhou, L.; Xia, Y.; Brownjohn, J.; Koo, K. Temperature analysis of a long-span suspension bridge based on field monitoring and numerical simulation. *J. Bridge Eng.* **2016**, *21*, 04015027. [[CrossRef](#)]
20. Lu, H.; Hao, J.; Zhong, J.; Wang, Y.; Yang, H. Analysis of sunshine temperature field of steel box girder based on monitoring data. *Adv. Civ. Eng.* **2020**, *2020*, 9572602. [[CrossRef](#)]
21. Mohan, K.; Sreemathy, J.; Saravanan, U. Numerical investigation into thermal load responses of steel railway bridge. *IOP Conf. Ser. Earth Environ. Sci.* **2017**, *80*, 012042. [[CrossRef](#)]
22. Gu, B.; Xie, F.; Lei, L.; Gao, W. Computational method for 3D sunshine temperature field of long-span bridge structures. *J. Southeast Univ. Nat. Sci. Ed.* **2019**, *49*, 664–671. (In Chinese)
23. Lu, Y.; Li, D.; Wang, K.; Jia, S. Study on solar radiation and the extreme thermal effect on concrete box girder bridges. *Appl. Sci.* **2021**, *11*, 6332. [[CrossRef](#)]
24. Wang, Y.; Zhan, Y.; Zhao, R. Analysis of thermal behavior on concrete box-girder arch bridges under convection and solar radiation. *Adv. Struct. Eng.* **2016**, *19*, 1043–1059. [[CrossRef](#)]
25. Lou, P.; Zhu, J.; Dai, G.; Yan, B. Experimental study on bridge-track system temperature actions for Chinese high-speed railway. *Arch. Civ. Mech. Eng.* **2018**, *18*, 451–464. [[CrossRef](#)]
26. Shi, T.; Zheng, J.; Deng, N.; Chen, Z.; Guo, X.; Wang, S. Temperature load parameters and thermal effects of a long-span concrete-filled steel tube arch bridge in Tibet. *Adv. Mater. Sci. Eng.* **2020**, *2020*, 9710613. [[CrossRef](#)]
27. Gottsäter, E.; Ivanov, O.L.; Miklós, M.; Plos, M. Validation of temperature simulations in a portal frame bridge. *Structures* **2018**, *15*, 341–348. [[CrossRef](#)]
28. Yan, B.; Cheng, R.; Xie, H.; Zhang, X. Vertical nonlinear temperature gradient and temperature load mode of ballastless track in China. *Mathematics* **2022**, *10*, 120. [[CrossRef](#)]
29. Wang, J.; Fang, Z. Temperature variation of concrete box girder bridge. *J. Hunan Univ. Nat. Sci.* **2008**, *4*, 23–28. (In Chinese) [[CrossRef](#)]
30. Hu, Q.; Gao, M.; Wang, S.; Zhang, J. Calculating and using solar radiation in Qinghai-Tibet Plateau. *J. Lanzhou Jiaotong Univ.* **2005**, *4*, 62–66. (In Chinese)
31. Li, R.; Yang, W.; Ji, G.; Zhao, J. Parameterization of effective radiation over the Qinghai-Tibet Plateau. *Acta Energ. Sol. Sin.* **2006**, *3*, 274–278. (In Chinese)
32. Jiang, X.; Li, Y. Climatological characteristics of surface radiation over the Tibetan Plateau. *Resour. Sci.* **2010**, *32*, 1932–1942. (In Chinese)